Formation of creep cavities in austenitic stainless steels

Junjing He[1],[*] and Rolf Sandström[1]

[1]*Materials Science and Engineering, KTH Royal Institute of Technology, 100 44 Stockholm, Sweden*

ABSTRACT

The possibility of creep cavity formation at subboundaries in austenitic stainless steels is analysed. It is demonstrated that such nucleation is thermodynamically feasible. A minimum stress must be exceeded in order to create cavities. The nucleation is assumed to take place where subboundaries on one side of a sliding grain boundary meet subgrain corners on the other side (double ledge models). Alternative cavitation positions can be found where particles meet subboundaries. The nucleation model can quantitatively predict the observed nucleation rate. The model gives a nucleation rate that is proportional to the creep rate in agreement with many experiments.

Introduction

Austenitic stainless steels are widely used for the high-temperature components of power plants, where creep strength and oxidation resistance are critical factors. Therefore, it is of utmost importance to understand the life controlling rupture mechanisms in these steels. Creep cavitation plays an important role during rupture of materials at high temperatures. Rupture proceeds with the formation, growth and coalescence of creep cavities along grain boundaries. Nucleation of cavities has been observed at a number of positions in the microstructure. The nucleation can take place at inclusions or second phase particles, at grain boundary ledges and other irregularities, and at grain boundary triple points. In particle free alloys, the nucleation often occurs at intersections between grain and subgrain boundaries [1–3]. In particle containing alloys, cavities nucleate at

particles on sliding grain boundaries [4–9]. A vast volume of research effort has been performed to explore the mechanisms of cavity nucleation. In spite of this, the nucleation mechanisms in individual alloys are still unclear in many cases. However, it is well established that creep cavities typically nucleate at grain boundaries due to Grain Boundary Sliding (GBS) [5–7, 9].

Harris [10, 11] proposed that cavities can nucleate at particles when the GBS rate is fast enough. In Harris' model, there exists a critical particle radius for cavity nucleation which is related to the GBS displacement rate. For smaller particles to initiate cavities, a higher GBS rate is required. With the help of models for GBS that have recently been developed [4], it has been possible to make quantitative predictions. By combining the GBS models with Harris' model, He and Sandström [4] modelled cavity nucleation at particles. The predicted number of

cavities nucleating at particles showed a good agreement with the experimental number of cavities.

Lim [1] proposed that cavities can nucleate at intersections of subgrains and grain boundaries and he developed a grain boundary dislocation (GBD) pile up model. The total number of dislocations in the pile up is considered to generate the steady state stress concentration. In this case, there is no incubation time for cavity nucleation since the GBD pile up is a steady state phenomenon of the secondary creep. However, a threshold stress is necessary, below which cavities will not be formed. By deriving the formation energy for cavities, he concluded that this was thermodynamically feasible for cavity nucleation at substructures for the metals that he studied, for example copper.

Sandström and Wu [3] developed a strain controlled model that can predict the cavity nucleation behaviour quantitatively. They proposed that cavities can nucleate at ledges or subboundary intersections due to GBS. The grain boundaries are assumed to have randomly distributed ledges or other inhomogeneities with a typical spacing. Here a detailed derivation of the model will be given for the first time. The basic assumption in the model is that the grain boundaries consist of two closely spaced layers and that cavities are nucleated when an inhomogeneity on one layer meets one on the other layer. The model is referred to as the double ledge model. The model results are in the same form as the experimental observations, namely that the nucleation rate is proportional to the creep rate.

The aim of this paper is to propose models for cavity nucleation at intersections of subboundaries with grain boundaries for austenitic stainless steels based on the GBS models introduced in [4]. The modelling results will be compared with experimental data for different types of austenitic stainless steels.

Grain boundary sliding model

As mentioned above, creep cavity formation is related to GBS. Two GBS models have been presented by He and Sandström [4] for austenitic stainless steels, of which the shear sliding model will be introduced here since it is of more general nature. In the shear sliding model, the GBS displacement rate v_{sd} is proportional to the creep rate $\dot{\varepsilon}$ by a parameter C_s:

$$v_{sd} = \Phi \frac{3}{2} \frac{d_{grain}}{\xi} \dot{\varepsilon} = C_s \dot{\varepsilon}, \tag{1}$$

where Φ is the fractional contribution of the GBS to the total displacement rate. The Φ value was found to be dependent only on the stress exponent n. The value of Φ is in the range from 0.1 to 0.33 when the stress exponent n varies from 1 to infinity. Φ is approximately 0.23 for austenitic stainless steels when the creep stress exponent is in the range of 5–10 [4, 12, 13]. ξ is a factor that relates the hexagonal grain size to the measured grain size d_{grain}, which is approximately 1.82 [14].

$$\xi = \frac{d_{grain}}{a_{hex}} = \sqrt{\frac{6}{\pi \tan(\pi/6)}} \approx 1.82, \tag{2}$$

where a_{hex} is the length of the side of the hexagons. Finally, the parameter C_s is dependent on the grain size.

It has been shown that there is an initial stage for the GBS displacement, where the GBS rate is higher. However, by taking the initial GBS displacement into account, the modelling results of C_s still show a good agreement with the average value of the experimental data for austenitic stainless steels [4]. The results will be used here in the development of cavity nucleation models in "Number of creep cavities formed at subboundaries" Section.

Thermodynamics of cavity nucleation at subboundaries

Experimentally, it has been found that the number of cavities is approximately proportional to the creep strain. The nucleation rate can be expressed as

$$\frac{dn}{dt} = B\dot{\varepsilon}_{cr}, \tag{3}$$

where B is a constant and $\dot{\varepsilon}_{cr}$ is the creep strain rate. This relation was experimentally first observed by Needham et al. for copper [15] and for austenitic stainless steels [16]. This relation has also been used for example for copper by Sandström and Wu [3], and for alumina by Page and Lankford [17]. In this work, a model based on cavity nucleation that gives a similar form to Eq. (3) will be proposed. Models about cavity formation at intersections of subboundaries with grain boundaries will be introduced. However, before we proceed to the cavity nucleation

models, it will be analysed whether it is possible for cavities to nucleate at subboundaries in austenitic stainless steels.

Gibbs energy model for cavity nucleation at subboundaries

Lim [1] proposed a GBD pile up model which can be used to check whether it is thermodynamically feasible for cavity nucleation at subboundaries. In Lim's model, high stress concentrations are generated by pile ups of GBDs. In this case, the pile ups of GBDs are part of the steady-state creep process, so the high stresses do not relax. Now the thermodynamic feasibility for formation of creep cavities will be examined.

In the model, it is assumed that the cavities can be formed by consuming part of the GBDs' energy. So the cavity formation can gain energy from the following 3 parts.

1. Part of the line energy of the GBD is consumed ΔG_1

$$\Delta G_1 = \frac{\mu b^2}{2\pi(1-v)}\ln\left(\frac{R_{cut}}{r_0}\right)\int_{r_0}^{r\sin\alpha}\sqrt{(r\sin\alpha)^2-x^2}\,\Psi(x)\mathrm{d}x,$$

(4)

where μ is the shear modulus, b is the Burgers' vector, v is the Poisson's ratio and x is the coordinate along the grain boundary. r_0 and R_{cut} are the core and cut-off radius of the dislocations, r is the radius of the curvature and α is half the tip angle of the lenticular shaped cavities. $\Psi(x)$ is the GBD density function, see Eq. (8) below.

2. The interaction energy among the consumed GBDs, as well as between the remaining and consumed GBDs ΔG_2

$$\Delta G_2 = \frac{\mu b^2}{\pi(1-v)}\ln\left(\frac{R_{cut}}{r_0}\right)\int_{r_0}^{r\sin\alpha}\sqrt{(r\sin\alpha)^2-x^2}$$

$$\left\{\int_{x+r_0}^{x+R_{cut}}\Psi(x')\ln\left(\frac{R_{cut}}{x'-x}\right)\mathrm{d}x'\right\}\Psi(x)\mathrm{d}x.$$

(5)

3. The strain energy of the remaining GBDs over the volume taken up by the cavity and its surroundings ΔG_3.

$$\Delta G_3 = F_v'r^3\int_{r\sin\alpha}^{r\sin\alpha+R_{cut}}\frac{1}{2G}\left(\frac{\mu b}{2\pi(1-v)}\frac{1}{x}\right)^2\Psi(x)\mathrm{d}x,$$

(6)

where $F_v = 2\pi/3(2 - 3\cos\alpha + \cos^3\alpha)$, $F_v' = 1.5\,F_v$. F_v and F_v' are dimensionless functions. F_v when

multiplied by r^3 gives the volume consumed by the cavity. When F_v' is multiplied by r^3 it gives the volume within which the strain energy is relaxed on the formation of the cavity [1].

The change in Gibbs energy on the formation of a cavity with radius of curvature r can be expressed as

$$\Delta G_{total} = -r^3F_v\sigma_{appl} + r^2F_s\gamma_s - r^2F_{GB}\gamma_{GB} - (\Delta G_1 + \Delta G_2 + \Delta G_3),$$

(7)

where γ_s and γ_{GB} are the surface and grain boundary energy per unit area. As explained before, when F_v is multiplied by r^3 it gives the volume consumed by the cavity. Similarly F_v, F_s and F_{GB} are also dimensionless functions which when multiplied by r^2 give the surface area and the grain boundary area consumed by the cavity. $F_s = 4\pi(1 - \cos\alpha)$ and $F_{GB} = \pi\sin^2\alpha$ [1]. In Eq. (7), the first term represents the work done by the applied stress on the system, and the second and the third term indicate the change in the surface and grain boundary energies. The fourth term, which is the sum of ΔG_1, ΔG_2 and ΔG_3, is the change of the GBDs pile up energy, which is also the energy gained by the cavity formation.

It is assumed that the GBDs form a double-end pile up, where the density function of the GBDs in the pile up can be represented by a dislocation density function $\Psi(x)$

$$\Psi(x) = \frac{\eta L}{\pi}\frac{1}{\sqrt{Lx-x^2}} - \frac{2(1-v)\sigma_{appl}}{\mu b\sin\theta}\frac{x-L/2}{\sqrt{Lx-x^2}}$$

(8)

where μ is the shear modulus, b is the Burgers' vector, σ_{appl} is the applied stress, x is the coordinate along the grain boundary, θ is the orientation of the dislocations in the pile up; for $\theta = \pi/2$ and $\theta = 0$, it corresponds to the climb and glide of dislocations along the grain boundaries respectively [18]. η is the average linear density of GBD, which is the number of dislocations per unit length of the grain boundary, see Eq. (11) below. L is the length of the pile up, which can be taken as the subgrain size d_{sub}. The subgrain size can be related to

$$d_{sub} = \frac{K\mu b}{\sigma},$$

(9)

where μ is the shear modulus, b is the Burgers' vector, σ is the applied stress, K is a constant and for austenitic stainless steels $K \approx 20$, which will be shown in the later part. By integrating the dislocation density

function, one can get the total number of dislocations N_{GBD} in the pile up.

$$N_{GBD} = \int_0^{d_{sub}} \Psi(x) dx. \tag{10}$$

Lim [1] developed an expression for the constant η, where he described that the value of η can be obtained from a reference state for the linear density of GBDs. Sandström et al. [18] refined this results, where the constant η can be expressed as

$$\eta = C_\eta \frac{\sigma T}{\mu} \left[\log \left(\frac{\Omega L^3}{b^3 \sin\theta} \frac{\dot{\varepsilon}(T,\sigma)}{4\delta D_{GB}} \right) + \frac{\Delta G_v}{k_B T} \right], \tag{11}$$

where C_η is a constant which is about 2×10^6 $(mK)^{-1}$, θ is the orientation of the dislocations in the pile up relative to the grain boundary, k_B is the Boltzmann constant, Ω is the atomic volume, δD_{GB} is the grain boundary diffusion coefficient and ΔG_v is the formation energy of vacancies. In the next subsection, the results of the energy changes by forming cavities will be shown.

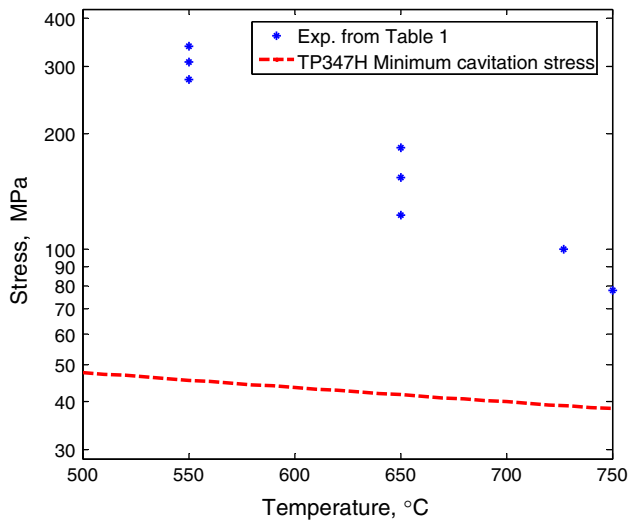## Results for cavity formation energies

With Eqs. (4)–(11), one can get the Gibbs energy change ΔG when forming the cavities. If ΔG is negative, energy is gained by forming a cavity, so cavity nucleation is feasible. The constants used to calculate the energy changes ΔG are listed in Table 2. Figure 1 shows the results for ΔG of TP347H austenitic stainless steels at temperatures of 550 and 750 °C.

Gain in Gibbs energy by forming a cavity indicates that the formation of cavities is thermodynamically feasible. The absolute value of ΔG increases with increasing cavity radius and applied stress, which indicates that the cavity formation occurs more readily at higher applied stress. Similar results have been obtained for other types of austenitic stainless steels, like TP304, TP321 and TP316 in our analysis. There is a threshold stress value below which cavities will not be formed. It can also be obtained from the models described above. The minimum cavitation stress corresponds to the value $\Delta G = 0$. As shown in Fig. 1b at conditions of 50 MPa and 750 °C, the $\Delta G = 0$ value shows increasing trend and close to 0, which means that it is close to the minimum cavitation stress. The results for the minimum cavitation stress are shown in Figs. 2 and 3 as a function of temperature. The minimum cavitation stress is modelled based on obtaining the ΔG value near a
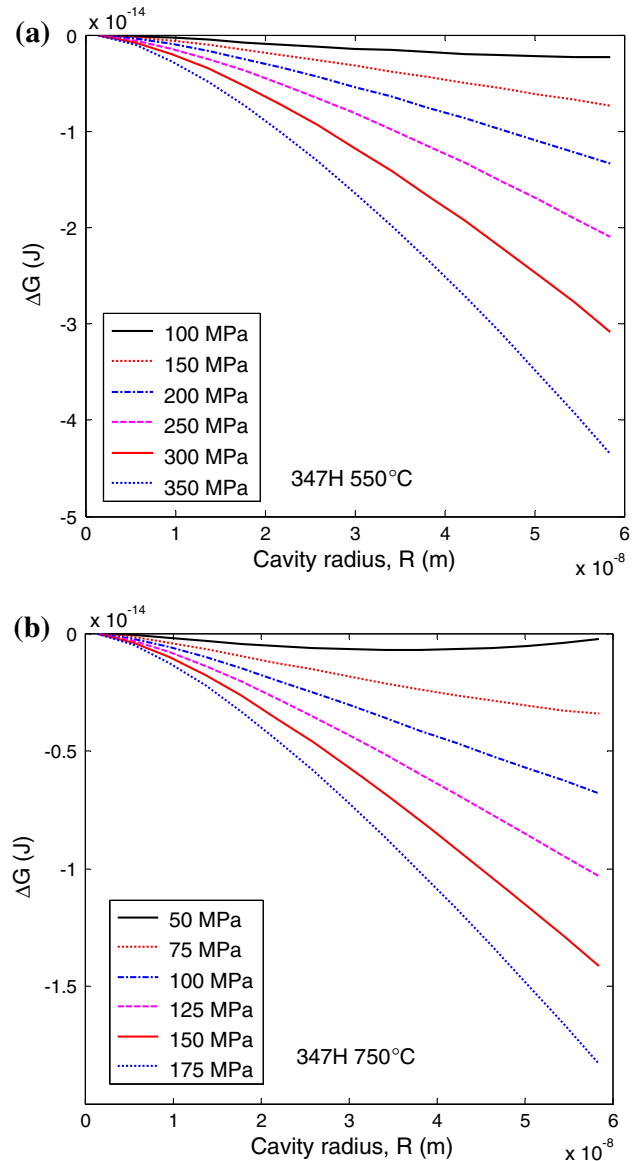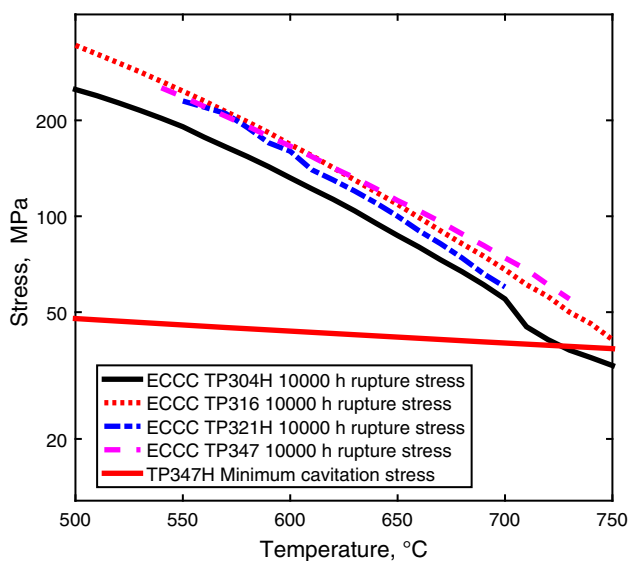

Figure 1 Change of Gibbs energy when a cavity is formed versus cavity radius for TP347H austenitic stainless steels at different stresses, **a** at 550 °C, **b** at 750 °C.

small cavity radius, which is about 100 b (where b is the magnitude of the Burgers' vector). As suggested by Lim [1], initially the cavity attains a size of about 100 b, which is rather precisely the minimum radius of a cavity nucleus. The experimental conditions considered in this work for the modelling of cavity nucleation at subboundaries are listed in Table 1. The minimum cavitation stress decreases with increasing of temperature. In Fig. 2, the modelled minimum cavitation stress is compared with observed cavitation [6, 9, 16, 19] which are listed in Table 1. It can be

Figure 2 Minimum cavitation stress versus temperature for TP347H austenitic stainless steels. Experimental data from Table 1 are used for comparison.

Figure 3 Minimum cavitation stress versus temperature for TP347H austenitic stainless steels. TP304H, TP316, TP321H and TP347 ruptured after 10,000 h from ECCC [21] are used for comparison.

easily seen that the modelled minimum cavitation stress is well below the applied stress in the experimental conditions where cavities have been observed. The modelled minimum cavitation stress for other austenitic stainless steels TP304H, TP321H and TP316H, show almost identical results. By comparing to the minimum cavitation stress, it can be seen that it is always thermodynamically feasible for cavities to nucleate at subboundaries in the current covered experimental cases since the experimental applied stress is well above the minimum cavitation stress required for cavity formation.
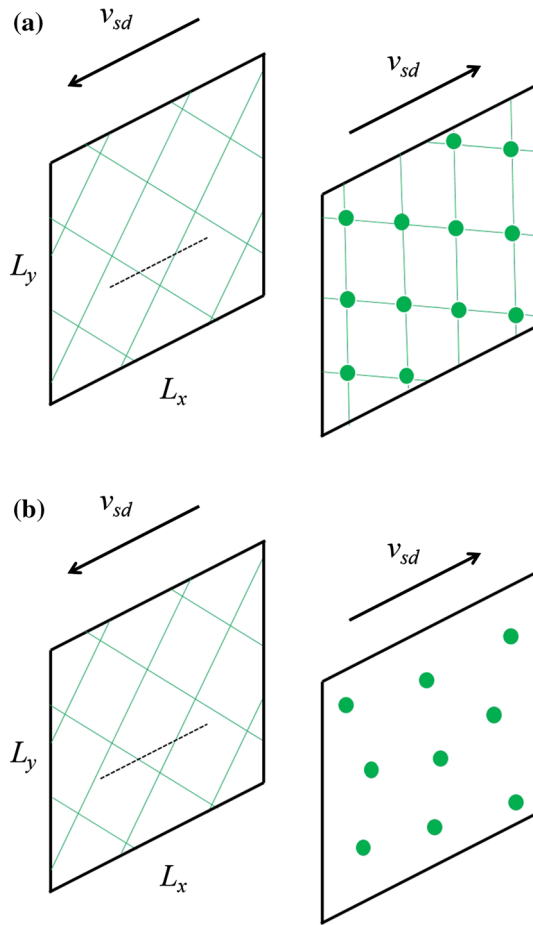
For comparison with a typical design stress, the stress giving rupture in 10,000 h (a little more than a year) is given. As shown in Fig. 3, the minimum cavitation stress is in general well below a typical design stress; in this case, the cavitation stress is in the range 35–50 MPa for temperatures between 500 and 750 °C.

Number of creep cavities formed at subboundaries

Model for nucleation frequency

Sandström and Wu [3] developed a double ledge model that gives a relation of the type in Eq. (3) and can predict the cavity nucleation behaviour quantitatively. They proposed the mechanism that cavities nucleate at subboundary intersections due to GBS. Here a detailed derivation of the model will be given. In the previous section, it was shown that it is thermodynamically feasible for cavity nucleation at subboundaries. Here the double ledge model will be used to quantify the cavity nucleation at subboundaries due to GBS. Figure 4a shows the intersection of subboundaries with subboundary corners on a sliding grain boundary with an area of $L_x \times L_y$, and sliding velocity of v_{sd}. When the particles or

Table 1 Temperature and stress conditions for observed creep cavitation

Material	Temperature (°C)	Stress (MPa)	Test time (h)	Reference
TP304XX	750	78	460–5100	[19]
TP347XX	750	78	460–5100	[6]
TP304	727	100	250	[9]
TP347	550	277–338	154–1660	[16]
TP347	650	123–184	160–2170	[16]
TP304	700	63.1	150	[20]

Figure 4 **a** Intersections of subboundaries with subboundary corners on the opposite side of a sliding grain boundary, **b** Intersections of subboundaries with particles on a sliding grain boundary.

subboundary corners meet the subboundaries on the other side of a sliding grain boundary, cavities will be formed. It is assumed that only the steep angle (formed by the grain boundary intersect with the sliding direction) will be effective for cavity nucleation. The number of subboundary corners per unit grain boundary area can be expressed as

$$n_{\mathrm{cor}} = \frac{1}{d_{\mathrm{sub}}^2},$$ (12)

where d_{sub} is the subgrain size. The sliding area of subboundary corners during GBS in time dt is

$$dA = L_y \frac{L_x}{d_{\mathrm{sub}}} v_{\mathrm{sd}} dt.$$ (13)

In the model, it is assumed that cavity nucleation takes place when the subboundary on one side of a

sliding grain boundary meets the subboundary corners on the other side of the grain boundary. The number of subboundary/subboundary corners meet N_{s} can be expressed as

$$N_{\mathrm{s}} = dA n_{\mathrm{cor}}.$$ (14)

This is the number of nucleation sites for cavities. Then one can obtain the number of cavities per unit area as

$$n_{\mathrm{cav}} = \frac{N_{\mathrm{s}}}{L_x L_y} = \frac{v_{\mathrm{sd}} dt}{d_{\mathrm{sub}}^3}.$$ (15)

By combining Eqs. (1) and (15), one finds the cavity nucleation rate at intersections of subboundary/subboundary corners:

$$\frac{\mathrm{d}n}{\mathrm{d}t} = \frac{C_{\mathrm{s}}}{d_{\mathrm{sub}}^3} \dot{\varepsilon}_{\mathrm{cr}},$$ (16)

where C_{s} can be obtained from the GBS model in "Grain boundary sliding model" Section.

For cavity nucleation at subboundary/particles intersections, there is a similar assumption that cavities can be generated when the subboundary on one side of a sliding grain boundary meets particles on the other side of the sliding grain boundary, as illustrated in Fig. 4b. In this case, a similar derivation can be made by replacing the subboundary corners with particles. Then one can get the cavity nucleation rate at subboundary/particles intersections:

$$\frac{\mathrm{d}n}{\mathrm{d}t} = \frac{C_{\mathrm{s}}}{d_{\mathrm{sub}} \lambda^2} \dot{\varepsilon}_{\mathrm{cr}},$$ (17)

where λ is the particle spacing.

For austenitic stainless steels, both particles and substructures can be expected to play an important role for cavity nucleation. Then by adding Eqs. (16) and (17), one can get the final result for cavity nucleation rate. The angle between the two subboundary nets lies in range of up to 45° since only steep angles are considered. By averaging over the angle range, it can be shown that a factor of 0.9 should be added (the details are not given here). So the final results for cavity nucleation rate are

$$\frac{\mathrm{d}n}{\mathrm{d}t} = \frac{0.9 C_{\mathrm{s}}}{d_{\mathrm{sub}}} \left(\frac{1}{\lambda^2} + \frac{1}{d_{\mathrm{sub}}^2} \right) \dot{\varepsilon}_{\mathrm{cr}} = B \dot{\varepsilon}_{\mathrm{cr}}.$$ (18)

When compared with Eq. (3), the final result Eq. (18) has the same form as the experimental observations namely that the cavity nucleation rate is proportional to the creep rate.

Constants used in the model

The constants used in this work are shown in Table 2.

The temperature dependence of the shear modulus μ for austenitic stainless steels is shown in Fig. 5. The linear fit (Equation listed in Table 2) of the shear modulus for austenitic stainless steels gives a good representation of the experimental values.

According to Eq. (9), the subgrain size is related to the applied stress. Equation (9) is compared to experimental data in Fig. 6. For austenitic stainless steels $K \approx 20$ fits well to the experimental data.

Comparison to experimental data

For formation of creep cavities, both subboundary corners and particles are taken into account, Eq. (18), which is related to the GBS parameter C_s, subgrain size d_{sub}, and particle spacing λ. The parameter C_s can be obtained from the GBS model as described above. The subgrain size is found from Eq. (9) and Fig. 6. The average value of particle spacing was derived in [4]. For the particles with radii in the range of 0.2–1 μm in the experimental results, the ratio of particle spacing/particle radius was approximately 7 [4].

Figure 7 shows the comparison of the experimental and modelling number of cavities per unit grain boundary area as a function of creep strain. The experimental conditions are listed in Table 1. More

detailed information can be found in references [6, 9, 16, 19]. Four sets of results are shown: TP347 at 550 and 650 °C [16], TP304 at 727 °C [9] and TP304XX at 750 °C [6, 19]. The model results corresponding to two of the sets (TP347 at 650 °C and TP304 at 727 °C) are in good agreement with the observation showing a maximum deviation of a factor of three. The data set (TP304XX at 750 °C) shows a lot of scatter. Although the model values lie inside the range of the
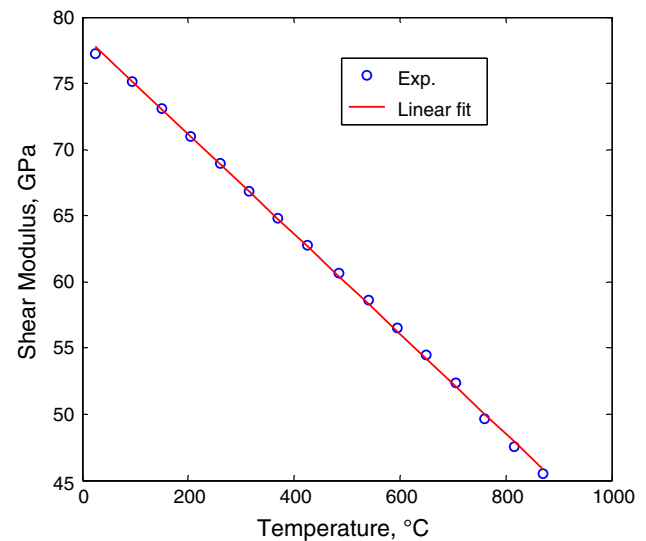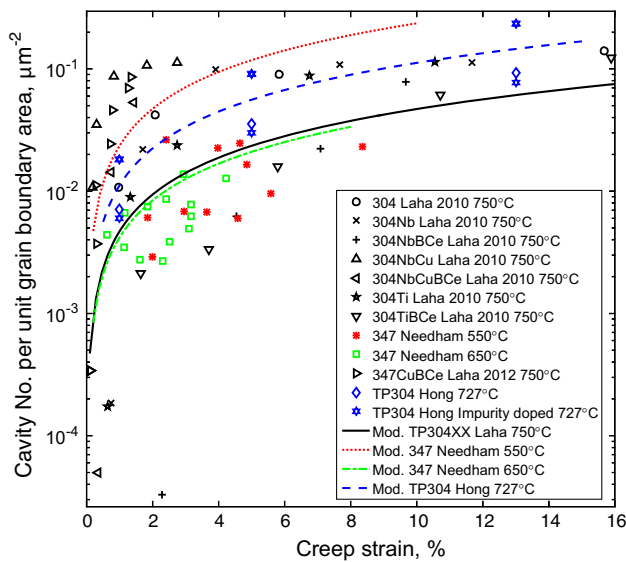

Figure 5 Experimental and linear fit shear modulus versus temperature for austenitic stainless steels. Experimental data from [23].

Table 2 Constants used in computations for austenitic stainless steels

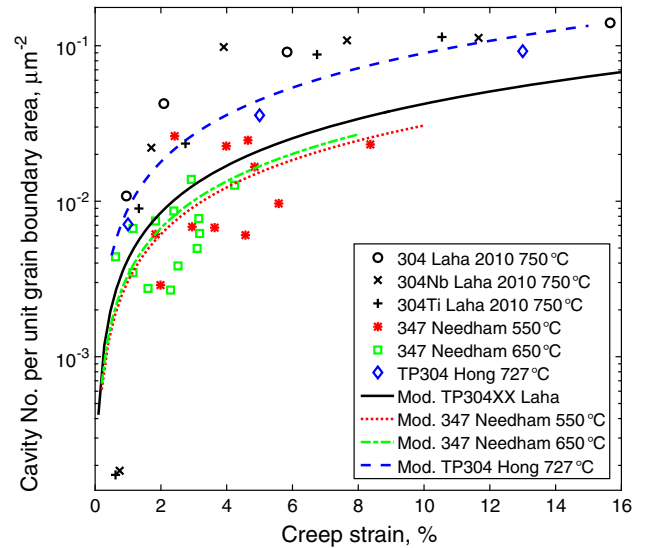| Parameter description	Parameter	Value	References
Grain boundary diffusion coefficient	δD_{GB}	$10^{-9.87} e^{\frac{-2.187e5}{R_{gas}T}}$	[22]
Shear modulus	μ	$(78 - 0.036 \times (T - 273)) \times 10^3$ MPa	[23]
Atomic volume	Ω	1.21×10^{-29} m^3	[24]
Boltzmann constant	k_B	1.381×10^{-23} J K^{-1}	
Creep exponent	n	5	[25]
Burger's vector	b	2.58×10^{-10} m	
Constant in expression for the subgrain size	K	20	This work Fig. 6
Surface energy per unit area	γ_s	2.8 J m^{-2}	[26]
Absolute temperature	T	K	
Poisson's ratio	ν	0.3	[27]
GBD core radius	r_0	$1.3\,b$	[28]
GBD cut-off radius	R_{cut}	$10^3\,b$	[29]
Tip angle of lenticular shaped cavity	α	20°	[1]
Grain boundary energy per unit area	γ_{GB}	0.8 J m^{-2}	[30]
Constant in the expression for η	C_η	2×10^6 (mK)$^{-1}$	[18]
Formation energy of vacancies	ΔG_v	2.47×10^{-19} J atom^{-1}	[31]
Orientation of dislocations in the grain boundary	θ	$\pi/4$	[1]
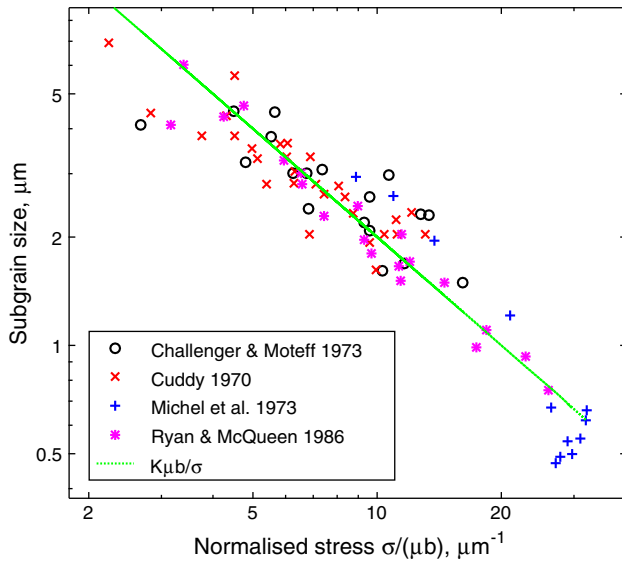
Figure 6 Subgrain size as a function of the normalised stress $\sigma/(\mu b)$. Experimental data from Challenger and Moteff [32] for TP316 steel, Cuddy [33] for TP304 steel, Michel et al. [34] for TP316 steel and Ryan and McQueen [35] for TP317 steel.

Figure 8 Modelling and experimental number of cavities per unit grain boundary area as a function of creep strain. Experimental data from, Hong and Nam [9] for TP304 steel, Laha et al. [19] for 3 different types of austenitic stainless steels, Needham and Gladman [16] for TP347 steel. The experimental conditions are listed in Table 1.

Figure 7 Comparison of modelling and experimental number of cavities per unit grain boundary area as a function of creep strain. Experimental data from [6, 9, 16, 19], the test conditions are listed in Table 1.

considered the modified results in Fig. 8 are obtained. The model values for the other data sets in Fig. 8 are also modified in the same way, but this has only a small effect. With the modified results, also the model values for TP347 at 550 °C are well centred in relation to the experimental findings.
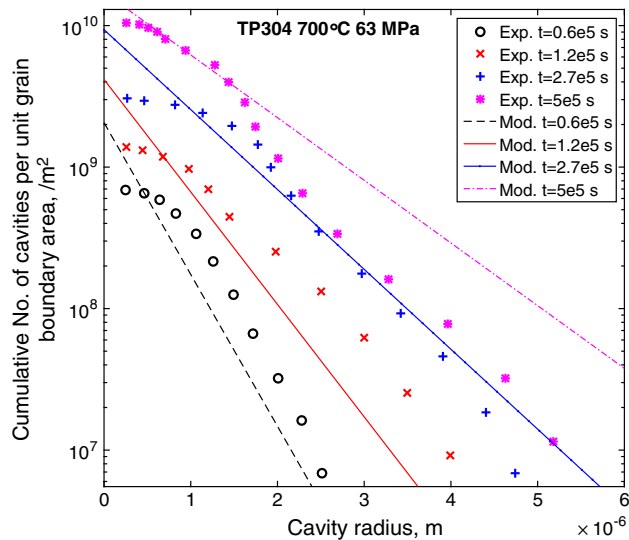
To further analyse the comparison between the model and the experiments, the data sets in Fig. 8 have been restricted to commercial steels. Steels with special additions are not considered. The number of cavities versus creep strain is given. Three of the data sets TP347 at 550 and 650 °C and TP304 at 727 °C are represented in quite a reasonable way by the model. For the fourth data set (TP304XX at 750 °C), the deviation between model and experiment is considerably smaller than in Fig. 7 although not satisfactory. The reason for the deviation for this data set is not known.

Discussion

Effect of cavity size distribution

The observation of the number of cavities per unit area is influenced by the cavity size distribution. Measured size distributions have been found in the

observations, a precise comparison is difficult to make.

For TP347 at 550 °C, it has to be taken into account that many cavities are quite small at this temperature and only the larger ones are recorded in the experiments. This is analysed in the discussion. If this is

Figure 9 Comparison of modelling and experimental cavity size distribution for TP304 austenitic stainless steels. Experimental data from [20]; the test conditions are listed in Table 1.

references [9, 20, 36]. Cumulative size distributions from [20] are shown in Fig. 9. It is apparent that the distributions are approximately exponential. This can also be shown to be the case for the distributions in [9, 36]. The cumulative distribution functions can be expressed as

$$g(r, t) = A \exp(-kr) \quad (19)$$

where $g(r, t)$ is the number of cavities at time t with radius larger than r. A is the total number of cavities independent of size that should be compared with the cavity nucleation models described above, Eq. (18). k is the slope of the distribution function. k is the inverse of the mean cavity radius r_m, $k = 1/r_m$. The mean cavity radius r_m can be obtained from cavity growth models [37, 38]. The authors will analyse and give details for the growth models in a forthcoming paper [39]. Figure 9 shows the comparison of the modelling and experimental cumulative cavity number density as a function of the cavity radius. The total number of cavities is predicted with Eq. (18) and the cavity radius with established growth models without involving any fitting parameters.

In Fig. 9, the distributions deviate from straight lines when the cavity radius is below 1 μm. This is an indication that all cavities are no longer recorded due to limitation in the instrumental resolution. Similar behaviour is found for the distributions from [9, 36].

This means that the contribution from smaller cavities is not fully accounted for. For TP347 at 550 °C, the corresponding full resolution limit was 0.5 μm. The number of cavities larger than 0.5 μm is only 15 % of the total number of cavities. This has been taken into account in the modification of the modelling results in Fig. 8. The smaller corrections for the other data sets have also been made. The reduction factors were 0.8 for TP347 at 550 °C and TP304 at 727 °C and 0.9 for 304XX at 750 °C.

Comparison of different models for cavity formation

Using the classical theory of nucleation, cavities are formed at grain boundaries by clustering of vacancies. As proposed by Smith and Barnby [40], a high stress concentration is necessary for the cavity nucleation. The high stress concentration can be developed at grain boundary ledges, grain boundary triple points and particles. It is suggested that the mechanisms for cavity nucleation at particles can be decohesion of particles from the matrix or particle fracture, where high stress concentrations are required. In most available models, a threshold stress and an incubation time have been considered as the critical conditions for cavity nucleation to occur [41, 42]. However, it has been found that the estimated threshold stress is orders of magnitude higher than the applied stress, and the required incubation time is longer than the time for stress concentrations to be relaxed. On the other hand, it is also suggested that cavities may be nucleated by breaking the local atomic bonds by the high stress concentration. However, it has been proved that the local stresses can never reach this level during creep conditions [43].

Unlike the classical theory for cavity nucleation, the model described here involves the pile up of GBDs, which is a steady state phenomenon of the secondary creep processing, so there is no incubation time concerned. Furthermore, the model describes the energy changes when forming a cavity from a thermodynamical point, where cavities will obtain energy by consuming part of the energy of GBDs. The modelling results of Figs. 1, 2, and 3 clearly show that it is thermodynamically feasible for cavity formation at subboundaries. The minimum cavitation stress here is well below the experimental applied stress and in general below the typical designed rupture

stress in 10,000 h from ECCC [21]. At higher temperatures, the minimum cavitation stress is close to the typical design rupture stress. The reason might be that it is more difficult to form cavities at the larger subgrains at low stresses and high temperatures.

Needleman and Rice [44] introduced a diffusion length over which stress concentrations are relaxed rapidly, and it is taken as a critical particle radius above which particles will nucleate cavities [45, 46]. In Jiang et al. review [46], they analysed a number of models about cavity nucleation at particles including improved models for the diffusion length. All the models proposed gave a critical radius of 10–20 μm for particles, which is much higher than in the experimental observations [4–9]. In the present work, for cavity formation at intersections of subboundaries and particles, the particle radii are based on the experimental observations.

The presented double ledge model gives a number of cavities that are proportional to the creep strain in good accordance with a number of published experimental investigations, for example in [3, 16]. A detailed comparison between modelling and experimental results is given in Figs. 7 and 8. For three of the four investigated data set a satisfactory agreement was obtained.

Conclusions

1. By calculating the energy change when forming a cavity, it has been shown that it is thermodynamically feasible for cavity nucleation at subboundaries without an incubation time involved. A threshold stress exists below which cavities will not form, which is lower than the applied stress in the current investigated experimental cases.

2. A model referred to as the double ledge model has been combined with a model for grain boundary sliding to describe the nucleation frequency of cavities at subboundaries. It is assumed that cavities are formed when subboundary corners or particles on one side of a sliding grain boundary meet subboundaries on the opposite side of the sliding grain boundary. This model is in the similar form of the experimental observations that the cavity nucleation rate is proportional to the creep strain rate. The

model can predict the number of cavities formed in austenitic stainless steels in a reasonable way.

Compliance with ethical standards

Conflict of interest The authors declare that they have no conflict of interest.

References

[1] Lim LC (1987) Cavity nucleation at high temperatures involving pile-ups of grain boundary dislocations. Acta Metall 35(7):1663–1673. doi:10.1016/0001-6160(87)90114-3

[2] Presland AEB, Hutchinson RI (1963–64) The effect of substructure on the nucleation of grain-boundary cavities in magnesium. J Inst Metals 92:264–269

[3] Sandström R, Wu R (2013) Influence of phosphorus on the creep ductility of copper. J Nucl Mater 441(1–3):364–371. doi:10.1016/j.jnucmat.2013.06.020

[4] He J, Sandström R (2016) Modelling grain boundary sliding during creep of austenitic stainless steels. J Mater Sci 51(6):2926–2934. doi:10.1007/s10853-015-9601-0

[5] Cui Y, Sauzay M, Caes C, Bonnaillie P, Arnal B (2014) Modeling and experimental study of long term creep damage in austenitic stainless steels. Proc Mater Sci 3:122–128. doi:10.1016/j.mspro.2014.06.023

[6] Laha K, Kyono J, Shinya N (2012) Copper, boron, and cerium additions in type 347 austenitic steel to improve creep rupture strength. Metall Mater Trans A 43(4):1187–1197

[7] Shin JK, Nam SW, Lee SC (2005) A study of nitrogen effect on the characteristics of creep-rupture in 18Cr-9Ni austenitic steels. Key Eng Mater 297-300:409–414

[8] Laha K, Kyono J, Sasaki T, Kishimoto S, Shinya N (2005) Improved creep strength and creep ductility of type 347 austenitic stainless steel through the self-healing effect of

boron for creep cavitation. Metall Mater Trans A 36:399–409

[9] Hong JH, Nam SW, Choi SP (1986) The influences of sulphur and phosphorus additions on the creep cavitation characteristics in type 304 stainless steels. J Mater Sci 21(11):3966–3976. doi:10.1007/PL00020267

[10] Harris JE (1965) An analysis of creep ductility of magnox Al80 and its implications. J Nucl Mater 15(3):201–207

[11] Harris JE (1965) Nucleation of creep cavities in magnesium. Trans Metall Soc AIME 233:1509

[12] Crossman FW, Ashby MF (1975) The non-uniform flow of polycrystals by grain-boundary sliding accommodated by power-law creep. Acta Metall 23(4):425–440. doi:10.1016/0001-6160(75)90082-6

[13] Ghahremani F (1980) Effect of grain boundary sliding on steady creep of polycrystals. Int J Solids Struct 16(9):847–862. doi:10.1016/0020-7683(80)90053-0

[14] Zhang J, Luévano AJ, Przystupa MA (1994) Microstructural models for quantitative analysis of grains and second-phase particles. Mater Charact 33(2):175–185. doi:10.1016/1044-5803(94)90081-7

[15] Needham NG, Wheatley JE, Greenwood GW (1975) The creep fracture of copper and magnesium. Acta Metall 23(1):23–27. doi:10.1016/0001-6160(75)90065-6

[16] Needham NG, Gladman T (1980) Nucleation and growth of creep cavities in a type 347 steel. Metal Sci 14(2):64–72

[17] Page RA, Lankford J (1983) Characterization of creep cavitation in sintered alumina by small-angle neutron scattering. J Am Ceram Soc 66(8):c146–c148. doi:10.1111/j.1151-2916.1983.tb10116.x/pdf

[18] Sandstrom R, Wu R, Hagstrom J (2016) Grain boundary sliding in copper and its relation to cavity formation during creep. Mat Sci Eng 651:259–268. doi:10.1016/j.msea.2015.10.100

[19] Laha K, Kyono J, Shinya N (2010) Suppression of creep cavitation in precipitation-hardened austenitic stainless steel to enhance creep rupture strength. Trans Indian Inst Met 63(2–3):437–441

[20] Chen I-W, Argon AS (1981) Creep cavitation in 304 stainless steel. Acta Metall 29:1321–1333

[21] ECCC (2005) European Creep Collaborative Committee DATA SHEETS 2005—HR3C.120

[22] Čermák J (1991) Grain boundary self-diffusion of 51Cr and 59Fe in austenitic NiFeCr alloys. Mater Sci Eng A 148(2):279–287

[23] Clark CL (1953) High temperature alloys (Hochwarmfeste Legierungen). Pitman Publishing Corporation, New York

[24] Arai M, Ogata T, Nitta A (1996) Continuous observation of cavity growth and coalescence by creep-fatigue tests in SEM. Jpn Soc Mech Eng 39(3):382–388

[25] NIMS creep data sheet for austenitic stainless steels. http://smds.nims.go.jp/creep/index_en.html

[26] Pitkänen H, Alatalo M, Puisto A, Ropo M, Kokko K, Vitos L (2013) Ab initio study of the surface properties of austenitic stainless steel alloys. Surf Sci 609:190–194. doi:10.1016/j.susc.2012.12.007

[27] 02 AHV (1991) Properties and selection: nonferrous alloys and special-purpose materials. ASM

[28] Wang R, Wang S, Wu X (2011) Edge dislocation core structures in FCC metals determined from ab initio calculations combined with the improved Peierls-Nabarro equation. Phys Scripta. doi:10.1088/0031-8949/83/04/045604

[29] Hirth JP, Lothe J (1982) Theory of dislocations, 2nd edn. Wiley, New York

[30] Rohrer GS, Holm EA, Rollett AD, Foiles SM, Li J, Olmsted DL (2010) Comparing calculated and measured grain boundary energies in nickel. Acta Mater 58(15):5063–5069. doi:10.1016/j.actamat.2010.05.042

[31] Schaefer HE, Maier K, Weller M, Herlach D, Seeger A, Diehl J (1977) Vacancy formation in iron investigated by positron annihilation in thermal equilibrium. Scr Metall 11(9):803–809. doi:10.1016/0036-9748(77)90079-5

[32] Challeger KD, Moteff J (1973) Quantitative characterization of the substructure of AISI 316 stainless steel resulting from creep. Metall Trans 4:749–755

[33] Cuddy LJ (1970) Internal stresses and structures developed during creep. Metall Trans 1:395–401

[34] Michel DJ, Moteff J, Lovell AJ (1973) Substructure of type 316 stainless steel deformed in slow tension at temperatures between 21 and 816 °C. Acta Metall 21:1269–1277

[35] Ryan ND, McQueen HJ (1986) Dynamic recovery and strain hardening in the hot deformation of type 317 stainless steel. Mater Sci Eng 81:259–272

[36] Arzate OR, Martinez L (1988) Creep cavitation in type 321 stainless steel. Mater Sci Eng A 101:1–6

[37] Beere W, Speight MV (1978) Creep cavitation by vacancy diffusion in plastically deforming solid. Met Sci 21(4):172–176

[38] Rice JR (1981) Constraints on the diffusive cavitation of isolated grain boundary facets in creeping polycrystals. Acta Metall 29:675–681

[39] He J, Sandström R (2016) Prediction of creep rupture strength for austenitic stainless steels. To be published

[40] Smith E, Barnby JT (1967) Crack nucleation in crystalline solids. Metal Sci J 1:56–64

[41] Raj R, Ashby MF (1975) Intergranular fracture at elevated temperature. Acta Metall 23(6):653–666. doi:10.1016/0001-6160(75)90047-4

[42] Raj R (1978) Nucleation of cavities at second phase particles in grain boundaries. Acta Metall 26(6):995–1006. doi:10.1016/0001-6160(78)90050-0

[43] Yoo MH, Trinkaus H (1983) Crack and cavity nucleation at interfaces during creep. Metall Trans A 14(3):547–561. doi:10.1007/BF02643772

[44] Needleman A, Rice JR (1980) Plastic creep flow effects in the diffusive cavitation of grain boudaries. Acta Metall 28(10):1315–1332

[45] Chokshit AH, Mukherjee AK (1989) An analysis of cavity nucleation in superplasticity. Acta Metall 37(11):3007–3017

[46] Jiang XG, Earthman JC, Mohamed FA (1994) Cavitation and cavity-induced fracture during superplastic deformation. J Mater Sci 29(21):5499–5514. doi:10.1007/BF00349941